Catalysis Science & Technology

Accepted Manuscript

ROYAL SOCIETY OF CHEMISTRY

www.rsc.org/catalysis

Journal Name

RSCPublishing

ARTICLE

Does the Multiply Bound Oxo Ligand Directly Participate in the B–H bond Activation by the High-Valent Di-Oxo-Molybdenum(VI) Complex? A Density Functional Theory Study

Cite this: DOI: 10.1039/xoxxoooooox

Received ooth January 2012,
Accepted ooth January 2012

DOI: 10.1039/xoxxoooooox

www.rsc.org/

Liangfang Huang,[§] Jiandi Wang,[§] Xiaoqin Wei, Haiyan Wei*

The reduction of organic substrates using high-valent oxo-transition metal complexes represents a new catalytic activity. In this study, we theoretically investigated the mechanism of catalytic reduction of amides, amines, nitriles and sulfoxides with boranes by the high-valent di-oxo-molybdenum(VI) complex MoO_2Cl_2. Our computational results reveal that reduction of sulfoxides with boranes catalyzed by MoO_2Cl_2 proceeds via a [2+2] addition pathway involving the B–H bond of the borane adding across the Mo=O bond to form a metal hydride intermediate, followed by elimination of new species HOBcat, accompanied with loss of the sulfide. The activation free energies of the turnover-limiting step is calculated to be 24.0 kcal/mol. By contrast, the borane additions to either amide or amine or nitrile proceed through an ionic outer-sphere mechanism, in which the substrates attack the boron center to prompt the heterolytic cleavage of B–H bond, generating an anionic molybdenum(VI) hydride paired with a borylated amide/amine/nitrile cation. Then, the activated organic substrates abstract a hydride from the molybdenum(VI) center to complete the catalytic cycle. The activation free energies of the turnover-limiting step along the ionic outer-sphere pathway are calculated to be ~22.7, 19.7 and 30.6 kcal/mol for benzamide, N-(diphenylmethylene)benzenamine, and benzonitrile, respectively. These values are energetically more favorable (~3– 8.0 kcal/mol) than the [2+2] addition pathway. Along the ionic outer-sphere pathway, the multiply bonded oxo ligand does not participate in the activation of the B–H bond. The ionic outer-sphere mechanism suggests that the high-valent di-oxo-molybdenum(VI) complex MoO_2Cl_2 acts as a Lewis acid in catalyzing reduction reaction and activation of B–H bonds.

Introduction

Hydroboration is a clean and highly stereospecific reaction for the laboratory synthesis of organoboranes, and has become a valuable synthetic technique in organic chemistry.[1] For many years, the hydroboration of deactivated boranes, such as HBcat (cat=catechol), has involved the use of transition metal catalysts, most often late transition metals such as Rh and Ir and low-oxidation state early metals such as Ti.[2-5] A recent development in X–H (X = Si, B, P, and H) bond activation using high-valent transition metal complexes as powerful catalysts for the reduction of organic substrates has received considerable attention.[6] A number of high-valent transition-metal complexes ($CpMoO_2Cl$, MoO_2Cl_2, $ReO_2I(PPh_3)_2$, $Re(O/NAr)Cl_3(PPh_3)_2$, $ReMeO_3$, $[RuN(saldach)(MeOH)]^+$ (saldach = N,N'-cyclohexan-diyl-bis(salicylideneimine), etc.) has taken advantage of this efficient strategy for X–H bond activation and as well as the reduction of aldehydes/ketones[7-10], imines,[11] amides,[12] esters,[13] sulfoxides[14] and pyridine N-oxides[15] to the corresponding alcohols, amines, sulfides and pyridines, with high yields and selectivity.

Mechanistically, the activation of X–H (X=H, Si, B, C, etc.) bonds by transition metal complexes in a low oxidation state is reported to involve an initial oxidative addition of the X–H bond to an unsaturated metal center (Scheme 1a), which affords a stable metal hydride. The organic substrate (e.g., ketone) then coordinates to the metal center and undergoes migratory insertion into the metal-hydride bond, followed by reductive elimination to give the substituted organic product.[16] The key mechanistic steps thus are oxidative addition, followed by the substrate coordination, migratory insertion, and reductive elimination. In contrast, a [2+2] addition mechanism was proposed for di-oxo rhenium(V) and molybdenum(VI) complexes in the activation of Si–H,[9,17,18] B–H,[14b-d] P–H,[19] and H–H[20] bonds. The first example of such a mechanism was illustrated to account for the high-valent di-oxo-rhenium(V)

complex $ReO_2I(PPh_3)_2$ catalyzed the hydrosilylation of carbonyl compounds by Toste and co-workers,[17] involving the activation of Si–H bond through its addition across Re=O bond in [2+2] manner to give a hydrido-oxorhenium(V) complex (Scheme 1b), followed by insertion of the organic substrate (e.g., ketone) into the metal-hydride bond and a retro-[2 + 2] addition of the alkoxide group attacking the silyloxium group, to produce silyl ether and regenerate the catalyst, $ReO_2I(PPh_3)_2$. The key mechanistic steps thus are [2+2] addition, followed by the substrate coordination, migratory insertion, and retro-[2+2] addition. Moreover, Wu and co-workers have theoretically investigated the mechanism of carbonyl hydrosilylation catalyzed by di-oxo-rhenium (V) complex $ReO_2(I)(PPh_3)_2$, and confirmed the [2+2] addition mechanism to be the preferred reaction pathway.[21]

Scheme 1. (a) The oxidative addition/migration/reductive elimination mechanism for catalytic reduction by low-valent transition-metal complexes, and (b) the [2+2] addition mechanism for catalytic reduction by high-valent oxo-transition metal complexes.

(a) Oxidative/migration/reductive elimination

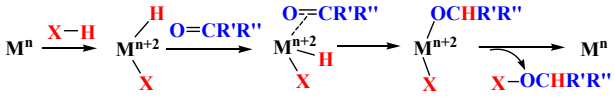

(b) [2+2] addition mechanism

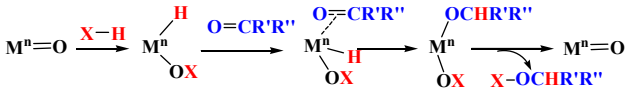

X=H, SiR_3, Bcat

These studies on the catalysis of high-valent transition-metal complexes represent an entirely new area for the catalytic reactivity of such complexes, in a total reversal of these complexes' role as oxidation catalysts.[22] A number of mechanistic studies, both experimental and theoretical, of high-valent transition-metal complexes catalyzed the reduction have been reported.[10,17,18,21,23] However, the prior computational work on high-valent transition metal complexes-catalyzed reduction reaction focused on the [2+2] addition mechanism, in which the multiply bonded ligands play an important role in assisting the X–H bonds activation.[21,23] Alternative mechanistic pathways were not investigated theoretically. In the present work, we report our computational results on the reduction of organic substrates with boranes by the high-valent di-oxo-molybdenum(VI) complex MoO_2Cl_2 (scheme 2). Our calculations indicate that the reduction of sulfoxides with boranes catalyzed by MoO_2Cl_2 proceeds via the [2+2] addition pathway, as shown in Scheme 1b, involving the B–H bond of the borane adding across the Mo=O bond to form a metal hydride intermediate, followed by elimination of a new species HOBcat, accompanied with loss of the sulfide. Whereas, a new mechanistic pathway – the ionic outer-sphere pathway is disclosed for the reduction of organic substrates of amides, amines, and nitriles by MoO_2Cl_2/boranes, in which the organic substrate attacks the boron center to prompt the heterolytic cleavage of B–H bond, generating an anionic molybdenum(VI) hydride paired with a borylated amide/amine/nitrile cation. To the best of our knowledge, there are relatively few well-characterized examples of B–H bond heterolytic cleavage by the transition metal complexes. Moreover, most of the heterolytic activation of B–H bond is characteristic of the cationic transition metal systems.[24,25] A closely related study is the recent report by Jagirdar and co-workers describing the heterolytic cleavage of B–H bonds by a cationic highly electrophilic ruthenium complex.[25] In this sense, the high-valent di-oxo-molybdenum(VI) complex MoO_2Cl_2 resembles the frustrated Lewis pairs (FLPs) recently popularized by Stephan and co-workers in catalyzing the reduction of organic substrates.[26] The ionic outer-sphere pathway involves the sequential transfer of a boryl/silyl cation and then a hydride to a polar double bond to furnish the reduction product. Along the ionic outer-sphere mechanistic pathway, the multiply bonded oxo ligand does not participate in the activation of the B–H bond. More importantly, the ionic outer-sphere mechanism does not involve the formation of a metal hydride intermediate, in contrast to oxidative addition mechanism, wherein an X–H bond adds to the metal center, or the [2+2] addition, wherein the X–H bond adds across the metal ligand bond. Both catalytic cycles are similar in their involvement of the metal hydride intermediate and its formation is taken as a rate-determining step. The theoretical investigation presented here provides a greater understanding of the activation of X–H bond by high-valent transition metal complexes, as well as useful information for future catalyst design.

Scheme 2. Catalytic reduction of organic substrates of amide, amine, nitrile and sulfoxide: benzamide ($PhC{=}ONH_2$), N-(diphenylmethylene)benzenamine (PhCPh=NPh), benzonitrile ($PhC{\equiv}N$), and diphenyl sulfoxide ($Ph_2S{=}O$) by MoO_2Cl_2/HBcat in this study.

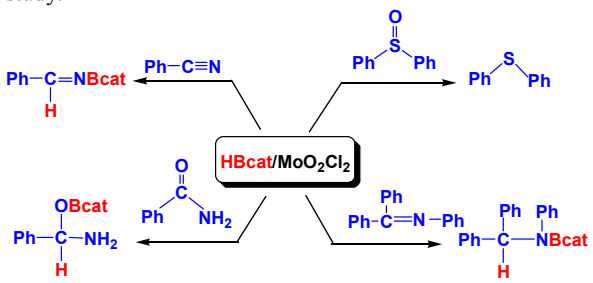

Computational Methods

All molecular geometries of model complexes were optimized using the M06 method level of DFT,[27] which was implemented in Gaussian 09.[28] The effective core potentials (ECPs) of Hay and Wadt with double-ζ valence basis sets (LanL2DZ) [29] were used to describe the Mo metal. In addition, polarization functions were added for Mo ($\zeta_f = 1.043$).[30] The 6-311G(d,p) basis set was used for all other atoms, such as B, C, H, O, S and Cl (BS1). All geometry optimizations were performed under solvent conditions using the SMD continuum model (an IEFPCM calculation with radii and nonelectrostatic terms for Truhlar and co-workers' SMD solvation model) [31] with THF as the solvent using tight convergence criteria, in order to properly describe the ionic outer-sphere process. In addition,

frequency calculations at the same level of theory were carried out to verify all stationary points as minima (zero imaginary frequencies) and transition states (one imaginary frequency). The transition states were further confirmed by calculating the intrinsic reaction coordinate routes toward the corresponding minima and reoptimizing from the final phase of IRC paths to reach each minima.

The final Gibbs energy values for ΔG reported in the current study were further refined by carrying out a single-point calculation on the basis of optimized geometries in solvent by using the same functional M06, but with the higher-level basis set, BS2, all-electron 6-311++G(2d,p) for nonmetal and quintuple zeta set with extra polarization basis sets (cc-QZVP) for molybdenum.[32] Detailed comparisons of different basis and methods are listed in Supporting Information. The CYLview molecular visualizing and manipulating program was employed to draw all the 3D molecular structures involved in this study.[33]

Results and Discussion

In the subsequent sections, the ionic outer-sphere pathway featuring the heterolytic cleavage of B–H bond upon the organic substrate nucleophilically attacks the borane atom in a borane metal complex is discussed first. Then, the [2+2] addition pathway in which the B–H bond initially adds across a meta-oxo bond to form a metal hydride intermediate is discussed.

Ionic outer-sphere mechanistic pathway: Previous research indicated that the ionic outer-sphere mechanism consists of three steps, [34,35] as shown in Scheme 3. First, the addition of borane to the metal center takes place, followed by nucleophilic attack of the organic substrate to prompt the heterolytic cleavage of the B−H bond, then hydride transfer to the activated organic substrate. In other words, the ionic outer-sphere pathway involves the sequential transfer of a boryl ion ($Bcat^+$) and then a hydride to a polar double bond to give the reduced product. Herein, we present the details of this mechanistic model in the investigation of B–H bond activation in boranes and the reduction of four organic substrates: benzamide ($PhC{=}ONH_2$), N-(diphenylmethylene)benzenamine (PhCPh=NPh), benzonitrile (PhC≡N), and diphenyl sulfoxide ($Ph_2S{=}O$) by the high-valent di-oxo-molybdenum complex MoO_2Cl_2. Figure 1 shows the free energy profiles for the reduction of four organic substrates with boranes catalyzed by di-oxo-molybdenum complex MoO_2Cl_2 (**1**). Optimized geometries of selected intermediates and transition states are shown in Figure 2 for benzamide (for optimized geometries with other organic substrates of N-(diphenylmethylene)benzenamine, benzonitrile, and diphenyl sulfoxide, see Supporting Information Figures S1a−S1c).

Scheme 3. The ionic outer-sphere mechanistic pathway for reduction of organic substrates with borane (HBcat) by the high-valent di-oxo-molybdenum complex MoO_2Cl_2 in this study.

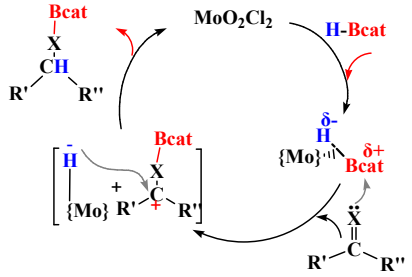

First Step: the addition of borane to the metal center. The first step is borane coordination to the molybdenum center forming a σ borane molybdenum complex **2**. Theoretical results reveal that **2** is in a weak end-on η^1-H(B) mode, with a significantly long Mo···H distance of 3.56 Å (see Supporting Information, Figure S1a). The borane molybdenum complex **2** is 10.6 kcal/mol less stable than catalyst MoO_2Cl_2 and HBcat.

Second step: The heterolytic cleavage of the B–H bond. Subsequent nucleophilic attack of organic molecules at the borane center in **2** forms a van der Waals species **3**. In the optimized geometry of van der Waals species **3** (Figure 2), benzamide oxygen, N-(diphenylmethylene)benzenamine nitrogen and benzonitrile nitrogen, diphenyl sulfoxide oxygen atom are calculated to be 2.41 Å, 2.77 Å, 2.42 Å and 2.84 Å away from the borane center, respectively. The formation of van der Waals species **3** is uphill in free energy by 19.0 kcal/mol for benzamide, 15.4 kcal/mol for N-(diphenylmethylene)benzenamine, 17.5 kcal/mol for benzonitrile and 20.0 kcal/mol for diphenyl sulfoxide. From the van der Waals species **3**, as we take either H···B or B···O(benzamide or diphenyl sulfoxide) or B···N(N-(diphenylmethylene)benzenamine or benzonitrile) separation as the reaction coordinate, heterolytic cleavage of the B–H bond occurs featuring a triple-well potential energy surface, comprised of two consecutive steps. The first step corresponds to the benzamide oxygen approaching the borane center, passing through the transition state **TS4**. In the optimized geometry of **TS4** (Figure 2), the benzamide oxygen binds to the borane center, with a B···O(C=O) distance of 2.12 Å, shorter by 0.29 Å than that in van der Waals species **3**. The vibrational mode corresponding to the imaginary frequency of **TS4** involves coupling of the benzamide oxygen to the borane center. **TS4** is an early transition state in the triple-well potential energy surface, which is energetically close to **3**.[36] The transition state **TS4** then evolves to the intermediate **4**, in which three moieties of borane, benzamide and the di-oxo-molybdenum complex are closely associated. The optimized geometry of **4** features the half-formation of the B−O(C=O) bond, with the B···O(C=O) distance being shortened to 1.48 Å from 2.41 Å in van der Waals species **3**, and half formation of the Mo−H bond, with Mo···H distance shortened to 1.91 Å from 3.33 Å in **3**. This is accompanied by half cleavage of the B–H bond, with B···H distance being elongated by 0.13 Å from a free borane molecule to 1.30 Å. The sum of the angles around the boron center in **4** is 336.2°, indicative of pyramidal sp^3 geometry, compared to 358.9° in HBcat, indicative of planar sp^3 geometry. We conclude that the coordination environment of HBcat is modified in **4** such that the geometry around the boron atom can be described as a tetrahedron structure

with the boron atom located at the center, which exhibits a *syn* S_N2-B reaction mode. Theoretical results reveal that **TS4** is associated with activation free energies of 17.2 kcal/mol (benzamide), 19.3 kcal/mol (N-(diphenylmethylene)benzenamine)), 23.4 kcal/mol (benzonitrile) and 21.3 kcal/mol (diphenyl sulfoxide). And intermediate **4** is 3.9 kcal/mol (benzamide), 4.0 kcal/mol (N-(diphenylmethylene)benzenamine), and 4.3 kcal/mol (diphenyl sulfoxide) lower than the corresponding transition state for each organic substrate. It is worth noting that with benzonitrile substrate, the PES has a very shallow minimum **4**, with the corresponding free energy being 0.5 kcal/mol higher than the transition state **TS4**. This result suggests that no stable intermediate **4** is formed along the reaction path. [37]

Cleavage of the B–H bond then occurs via the transition state **TS5**. In the optimized geometry of **TS5** (Figure 2), the length of the breaking B−H bond is 1.76 Å, which is elongated by 0.46 Å from intermediate **4**. Accompanied by cleavage of the B−H bond, the borane hydride transfers to the molybdenum center, (d(Mo–H) = 1.74 Å), which is 1.59 Å shorter than in van der Waals species **3.** The boryl moiety binds to the benzamide oxygen atom (d(B–O) = 1.41 Å), which is shortened by 1.00 Å as compared to van der Waals species **3**. Analytical frequency calculations confirmed that **TS5** is characterized by a borane hydrogen transferred to the molybdenum center. A full IRC analysis without symmetry restriction confirmed that **TS5** is the first-order saddle point that connects **4** and the intermediate **5**. Shown in Figure 2, the intermediate **5** is comprised of an anionic molybdenum hydride $[MoO_2(H)Cl_2]^-$ paired with a borylated benzamide ion $[PhCO(Bcat)NH_2]^+$, in which two moieties are separated with a significantly elongated B···H bond distance (3.56 Å). Theoretical results reveal that the B–H bond cleavage step (**TS5**) is associated with activation free energies of 15.9 kcal/mol (benzamide), 19.7 kcal/mol (N-(diphenylmethylene)benzenamine), 29.9 kcal/mol (benzonitrile) and 18.3 kcal/mol (diphenyl sulfoxide) from the reactants. The intermediate **5** was respectively calculated at 1.7 kcal/mol (benzamide), 6.2 kcal/mol (N-(diphenylmethylene)benzenamine), 1.4 kcal/mol (benzonitrile), and 8.0 kcal/mol (diphenyl sulfoxide) below **TS5**.

Combining the vibrational motion of the imaginary frequency in transition states **TS4** and **TS5** represents the expected normal mode of a *syn* S_N2-B reaction, which features the nucleophilic attack of organic molecules on the borane center. At the same time, the electrophilic borane hydrogen leaves the borane center to approach the molybdenum center, which results in simultaneous cleavage of the B–H bond and the formation of a Mo–H bond. As a consequence of the transformation from van der Waals species **3** into the ion pair **5**, natural bond order (NBO) charge analysis reveals that the migrating H atom of borane in **3** has a negative charge (-0.12 *e*). Accompanied by the B–H bond cleavage, the calculated NBO negative charge on the borane hydrogen decreases to -0.10 *e* in **TS5**, and to almost neutral in intermediate **5** (-0.02 *e*). Accordingly, the NBO charge trend on the borane center is reversed and becomes positively charged, i.e., 0.97 *e*, 1.07 *e* (**TS4**, **4**) →1.25 *e*, 1.29 *e* (**TS5**, **5**) during this step. When the electron density from borane effectively drains to the molybdenum center, the NBO charge on the molybdenum center becomes less positively charged, going from 1.09 *e* → 1.02 *e* → 0.92 *e*→ 0.88 *e*. The NBO charge trend with substrates of N-(diphenylmethylene)benzenamine (PhCPh=NPh), benzonitrile (PhC≡N), and diphenyl sulfoxide (Ph_2S=O) along **3** → **TS4**, **4** → **TS5**, **5** is similar with benzamide, see Supporting Information Table S2. Furthermore, We examined the heterolytic cleavage of H–B bond process in terms of frontier orbitals (Supporting Information Figure S2). Analysis showed that the interaction of the organic substrate with borane weakens the H–B σ bonding orbital, and facilitates the hydride transfer from borane to the molybdenum center.

Third Step: The hydride transfer. Once the borylated benzamide cation $[PhCO(Bcat)NH_2]^+$ is formed, it then abstracts a hydride on the anionic molybdenum hydride $[MoO_2(H)Cl_2]^-$ to form the final product, borylated phenylmethanamine, $PhCHO(NH_2)(Bcat)$, closing the catalytic cycle via the transition state **TS6** (Figure 2). The calculated migration transition state (**TS6**) shows one imaginary vibrational mode in which the hydrogen moves away from the molybdenum center, with a distance of d(H···Mo) = 1.80 Å, and gets closer to C atom at borylated benzamide cation $[PhCO(Bcat)NH_2]^+$ to form a new C–H bond, with a distance of *d*(H···C) = 1.59 Å. The transition state **TS6** is calculated at 8.5 kcal/mol (benzamide), 5.6 kcal/mol (N-(diphenylmethylene)benzenamine) and 2.1 kcal/mol (benzonitrile), higher than the intermediate **5**. Furthermore, the hydride transfer should occur easily because of the large thermodynamic driving force, with ΔG(5→6) calculated as 11.5 kcal/mol for benzamide, 24.1 kcal/mol for (diphenylmethylene)benzenamine), and 31.4 kcal/mol for benzonitrile.

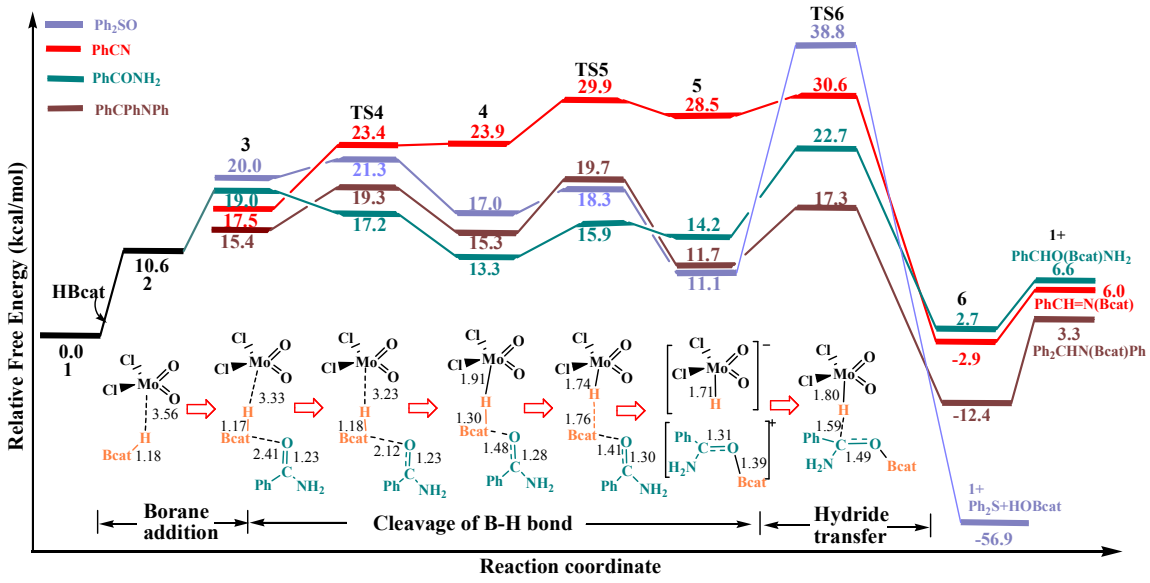

Figure 1. Schematic of the free-energy surface for the di-oxo molybdenum complex MoO_2Cl_2-catalyzed reduction of benzamide ($PhC{=}ONH_2$), N-(diphenylmethylene)benzenamine (PhCPh=NPh), benzonitrile ($PhC{\equiv}N$), and diphenyl sulfoxide ($Ph_2S{=}O$) with boranes via the ionic outer-sphere mechanistic pathway.

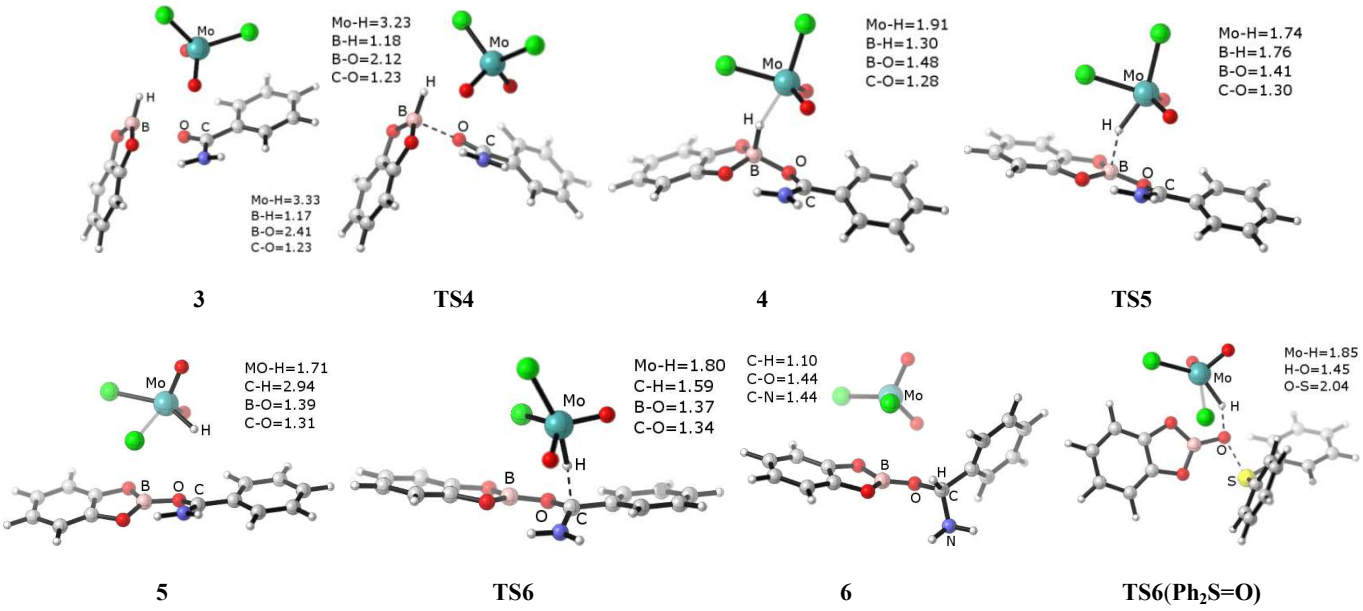

Figure 2. Calculated geometric structures along the heterolytic cleavage of B–H bond: **3→TS4→4→TS5→5→TS6→6** for MoO_2Cl_2-catalyzed hydroboration of benzamide ($PhC{=}ONH_2$), as well as the transition state **TS6($Ph_2S{=}O$)** corresponding to loss of thioether from the borylated diphenyl sulfoxide ion $[Ph_2SO(Bcat)]^+$ accompanied with elimination of a new species HOBcat.

However, for the sulfoxide substrate, unlike the hydride transfer to the C atom at the borylated benzamide cation $[PhCO(NH_2)(Bcat)]^+$ to form a new C−H bond via the transition state **TS6**, loss of thioether from the borylated diphenyl sulfoxide ion $[Ph_2SO(Bcat)]^+$ ion takes place when the hydride on the molybdenum moves to the sulfoxide oxygen atom, resulting in elimination of a new species, HOBcat. The corresponding transition state **TS6($Ph_2S{=}O$)** is calculated to require a much higher activation free energy (38.8 kcal/mol). In the optimized geometry of **TS6($Ph_2S{=}O$)** (Figure 2), the S···O distance increases to 2.04 Å, while the hydride leaves the molybdenum center (d(Mo···H) = 1.85 Å) and approaches the oxygen to form a H–O bond, with d(H···O) = 1.45 Å.

In summary, the high-valent di-oxo-molybdenum(VI) complex MoO_2Cl_2 catalyzes the reduction of organic substrates (benzamide, N-(diphenylmethylene) benzenamine, benzonitrile and diphenyl sulfoxide) with boranes along the ionic outer-sphere mechanistic pathway can be divided into three steps (Figure 1): (1) the addition

of borane to the metal, **1→2**, (2) the heterolytic cleavage of the B–H bond, **3→TS4→4→TS5→5**, and (3) the hydride transfer, **5→TS6**. Clearly, both the heterolytic cleavage step (**TS4** and **TS5**) and the hydride transfer step (**TS6)** have a comparatively higher barrier, of 17.2 kcal/mol, 15.9 kcal/mol and 22.7 kcal/mol for benzamide, 19.3 kcal/mol, 19.7 kcal/mol and 17.3 kcal/mol for N-(diphenylmethylene)benzenamine) and 23.4 kcal/mol, 29.9 kcal/mol and 30.6 kcal/mol for benzonitrile, implying that both steps can be the rate-determining step (RDS). Moreover, the hydride transfer step appears to be turnover-limiting in the case of diphenyl sulfoxide, due to the much larger activation free energy of **TS6(Ph$_2$S=O)**, 38.8 kcal/mol compared to that of the heterolytic cleavage step (**TS4**, **TS5**, 21.3 and 18.3 kcal/mol).

Furthermore, our theoretical results presented in Figure 1 showed that the heterolytic cleavage of the B–H bond in benzamide and N-(diphenylmethylene)benzenamine are significantly more efficient than in benzonitrile. This difference is due to electronic factors. The NBO charge on the nitrogen atom of van der Waals **3** for benzamide and N-(diphenylmethylene)benzenamine is −0.81*e* and −0.51*e*, respectively, which is more electron-donating than that with benzonitrile (−0.40 *e*). The more nucleophilic the organic substrate, the easier for the organic molecule approaching to the boron center, which in turn facilitate heterolytic cleavage of B–H bond.

The [2+2] addition pathway. In a [2+2] addition catalytic cycle, as shown in Scheme 1b, the activation of the X–H bond through its addition across one of the M=O bonds in a [2+2] manner was considered the first step, forming the metal hydrido intermediate[21,23] The reaction proceeds via migratory insertion of the organic substrates' double bond into the metal-hydride bond. Calhorda and Fernandes have reported on the activation of B–H bond and reduction of sulfoxides with boranes by high-valent rhenium complex $ReO_2(I)(PPh_3)_2$ and suggested the [2+2] addition mechanism to be the preferable pathway.[14c] Whereas, the reduction mechanism of organic substrates with boranes by high-valent molybdenum complex MoO_2Cl_2 via the [2+2] addition mechanism has not been conducted. In the following section, the reduction of organic substrates benzamide (PhC=ONH$_2$), N-(diphenylmethylene)benzenamine (PhCPh=NPh), benzonitrile (PhC≡N), and diphenyl sulfoxide (Ph$_2$S=O) by the high-valent di-oxo-molybdenum complex MoO_2Cl_2 are discussed in detail. Important structural parameters for intermediates and transition states calculated for the [2+2] addition mechanism with benzamide are summarized in Figure 3 (see Supporting Information Figures S3a−S3b for optimized geometries for the transition states and intermediates with N-(diphenylmethylene)benzenamine and benzonitrile). The energy profiles for the [2+2] addition mechanism for three organic substrates benzamide, N-(diphenylmethylene)benzenamine and benzonitrile catalyzed by MoO_2Cl_2 (**1**) are shown in Figure 4. The reduction of diphenyl sulfoxide (Ph$_2$S=O) with boranes by MoO_2Cl_2 is somewhat different and the details will be addressed in a separate section.

The [2+2] addition catalytic cycle begins with one molecule of HBcat across the Mo=O bond, via borane addition to one oxide, forming a new B–O bond and transfer of H(B) to molybdenum forming a Mo–H bond. The corresponding transition state is located at **TS7**. The optimized geometry of **TS7** consists of a four-member-ring (O2···B···H···Mo), (Figure 3) corresponding to simultaneously breaking the B–H bond (d(B···H) = 1.25 Å) while hydrogen abstraction by the molybdenum forms a Mo–H bond (d(Mo···H) = 2.05 Å) and the Bcat group bonds with the multiply bound oxygen to generate a B–O bond (d(B···O2) = 1.76 Å). The [2+2] addition transition state leads to generation of a molybdenum hydride intermediate **7** (MoO(OBcat)(H)Cl$_2$) (Figure 3), with a normal Mo–H bond distance of 1.67 Å. Theoretical results indicate that the [2+2] addition transition state is associated with an activation free energy of 27.6 kcal/mol. The resulting intermediate is 3.6 kcal/mol higher than the catalyst MoO_2Cl_2 and HBcat.

Following this [2+2] addition step, the molybdenum hydride intermediate then acts as the active species to reduce the organic substrate. First, an intermediate **8** (MoO(OBcat)(H)Cl$_2$(η^1-PhC=ONH$_2$) is formed with benzamide coordinated to the molybdenum center through oxygen atom. Then the reaction occurs through the insertion of benzamide into the Mo–H bond via **TS9** (Figure 3) to give a transition metal amine intermediate. The coordination geometry around molybdenum center in **8** can be viewed as a distorted octahedron with benzamide oxygen residing *trans* to one chloride ligand, with a significantly long Mo···O distance, at 2.20 Å, indicating the coordination of benzamide in **8** is in a much weaker end-on η^1 mode. The transition state **TS9** (Figure 3) features a four-member ring consisting of Mo–H and C=O bonds, in which the benzamide carbon atom approaches the molybdenum center with the H–C bond starting to form (1.36 Å) and the Mo–O distance decreases to 2.00 Å. The Mo–H distance considerably lengthens to 1.85 Å, together with C=O bond which is elongated to be halfway between a double and a single bond (1.33 Å). The calculated free energy barrier associated with the migratory insertion step (**TS9**) is moderate, 20.5 kcal/mol for benzamide and 18.1 kcal/mol for N-(diphenylmethylene)benzenamine. However, a significantly higher activation free energy of 33.8 kcal/mol is associated with benzonitrile. The insertion products, **9**, MoO(OBcat)(PhCHONH$_2$)Cl$_2$, MoO(OBcat)(PhCHPhNPh)Cl$_2$ and MoO(OBcat)(PhCH=N)Cl$_2$ are stable trigonal dipyramidal-coordinate complexes, and exergonic by 0.2 kcal/mol (benzamide), 14.1 kcal/mol (N-(diphenylmethylene)benzenamine), and 15.9 kcal/mol (benzonitrile).

The final step along the [2+2] addition catalytic cycle concerns the regeneration of catalyst, representing the transfer of the boryl group to the amine oxygen atom via a retro-[2 + 2] addition. The corresponding transition state **TS10** (Figure 3) is comprised of a four-member ring in which the B–O(PhCHO(NH$_2$)) distance decreases to 1.82 Å, and the Mo–O (PhCHO(NH$_2$)) distance lengthens to 1.98 Å. Theoretical results reveal that the transition state **TS10** is associated with activation free energies of 18.3 kcal/mol (benzamide), 16.8 kcal/mol (N-(diphenylmethylene)benzenamine), and 4.0 kcal/mol (benzonitrile(PhC≡N)). Elimination of the reduced product

(PhCHO(NH_2)(Bcat)) then regenerates the catalyst and completes the catalytic cycle.

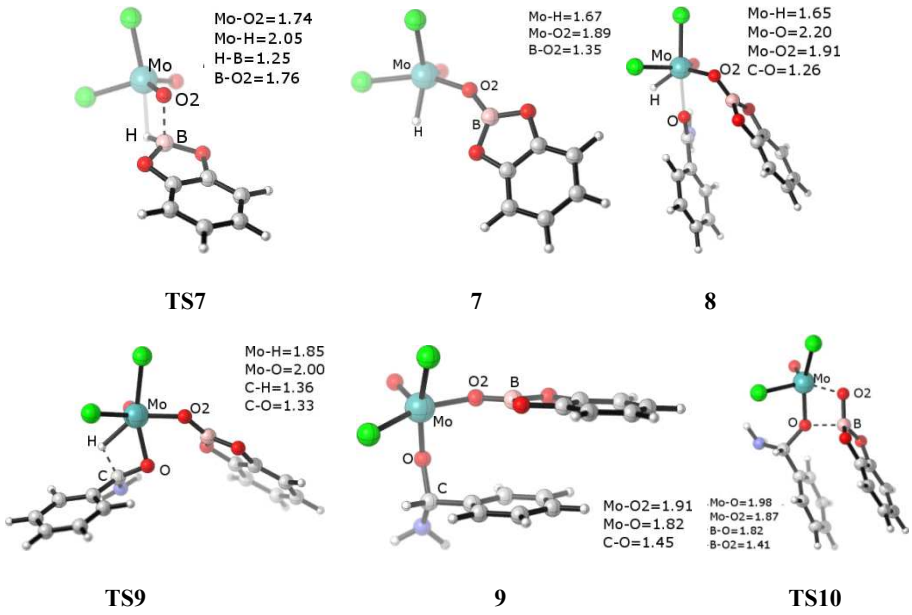

Figure 3. Calculated structures of transition states (**TS7**, **TS9**, **TS10**) and intermediates **7**, **8**, **9** for MoO_2Cl_2–mediated reduction of hydroboration of benzamide (PhC=ONH_2) with borane through the [2+2] addition pathway.

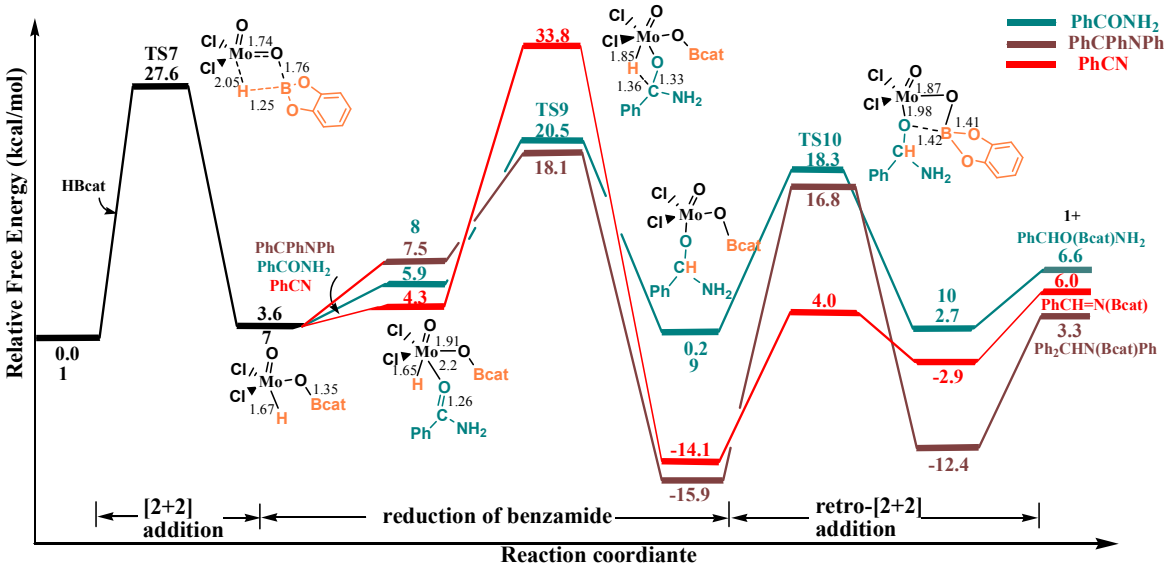

Figure 4. Schematic free-energy surface for the MoO_2Cl_2-mediated hydroboration of benzamide (PhC=ONH_2), benzonitrile (PhC≡N), N-(diphenylmethylene)benzenamine (PhCPh=NPh) through the [2+2] addition pathway.

In summary, the reduction of benzamide, N-(diphenylmethylene)benzenamine and benzonitrile and 1-(phenylsulfinyl)benzene with boranes mediated by the high-valent di-oxo-molybdenum(VI) complex MoO_2Cl_2 proceeds through the [2+2] addition mechanistic pathway are shown in Figure 4, our calculation indicated that with substrates of benzamide and N-(diphenylmethylene)benzenamine, the [2+2] addition transition state (**TS7**, 27.6 kcal/mol) is the rate-determing step. With substrate of benzonitrile, the highest activation free energy barrier corresponds to the migration insertion step and is associated with an activation free energy of 33.8 kcal/mol (**TS9**).

The [2+2] addition pathway for reduction of diphenyl sulfoxide (Ph_2S=O). The proposed [2+2] addition mechanism for reduction of sulfoxide with boranes by the high-valent di-oxo-molybdenum(VI) complex MoO_2Cl_2 is somewhat different from the mechanism described in Figure 4. Our computations predict a slightly lower activation energy for [2+2] addition of boranes adding across Mo=O bond in this case, starting from the sulfoxide complex, MoO_2Cl_2(Ph_2S=O), 24.0 kcal/mol (**TS11**). Thus, the sulfoxide complex, MoO_2Cl_2(Ph_2S=O)-catalyzed pathway should dominate under these conditions. It should be noted that this observation suggests that the reduction of a sulfoxide group with

boranes prefers the initial formation of a sulfoxide complex, which is consistent with the previous reported high-valent di-oxo-rhenium(V) complex by Calhorda and Fernandes.[14c] The optimized geometry of the transition state **TS11** (shown in the Supporting Information, Figure S4) is structurally similar to the previous located [2+2] addition transition state **TS7**, except for an additional Mo-(Ph_2S=O) bond. The transition state **TS11** possesses very similar bond lengths and angles, with a four-membered cyclic (O2···B···H···Mo) ring comprised of the forming Mo–H bond (2.11 Å) and the B–O2 bond (1.82 Å). The generated molybdenum hydride intermediate **11** is 0.3 kcal/mol more stable than the sum of the isolated reagents (MoO_2Cl_2 + HBcat + Ph_2SO).

Following the formation of molybdenum hydride intermediate, the reaction takes place in two steps: elimination of a new species HOBcat, followed by loss of the sulfide (Ph_2S) and regeneration of the catalyst. From the molybdenum hydride intermediate **11**, the proton on the Mo center transfers to the OBcat group to eliminate a species HOBcat via transition state **TS12**. The barrier for the transition state **TS12** is 18.2 kcal/mol relative to the molybdenum hydride intermediate **11**. In the optimized geometry of **TS12**, the H–O2 bond on Bcat has a bond length of 1.46 Å, and shows a quite long Mo−O2 bond of 2.14 Å, indicating dissociation of HOBcat. Elimination of species HOBcat leads to intermediate **12** ($MoOCl_2$(Ph_2S=O)), in which the metal has been reduced to Mo(IV). At this stage of the reaction, one molecule of Ph_2S has been released from Mo(IV) complex easily, with a barrier of 7.4 kcal/mol (**TS13**). During this process, owing to the loss of sulfide (Ph_2S), the metal has been oxidized back to Mo(VI), and the catalytic cycle is completed. In the optimized geometry of transition state **TS13** (Figure 5), the breaking S−O3 bond is 0.44 Å longer than that in a free sulfoxide. The free energies for reduction of sulfoxide with boranes along the [2+2] addition mechanism are summarized in Figure 6. And the highest activation free energy barrier corresponds to the [2+2] addition step, associated with an activation free energy of 24.0 kcal/mol (**TS11**).

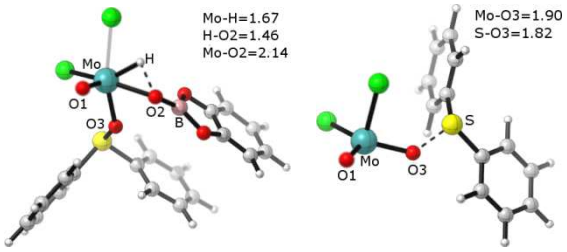

TS12 **TS13**

Figure 5. Calculated geometric structures of the transition states and the intermediates **TS12**, **TS13** along the [2+2] addition pathway for the MoO_2Cl_2-mediated reduction of diphenyl sulfoxide (Ph_2S=O) with borane.

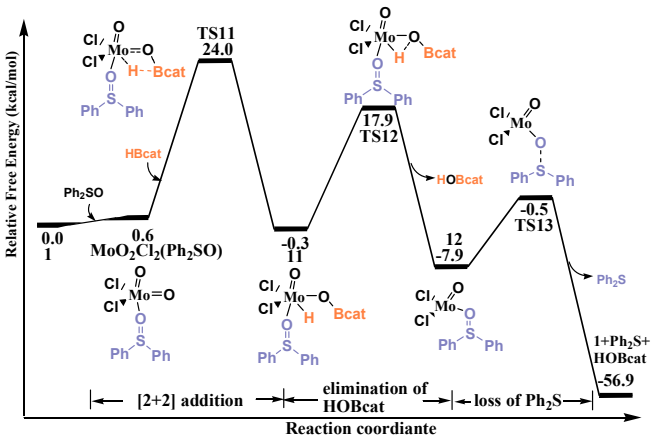

Figure 6. Schematic free-energy surface for the MoO_2Cl_2-mediated reduction of diphenyl sulfoxide (Ph_2S=O) with boranes through the [2+2] addition pathway.

From Figures 1, 4 and 6, we can see that, in the reactions of reduction of benzamide ($PhC{=}ONH_2$), N-(diphenylmethylene)benzenamine (PhCPh=NPh), and diphenyl sulfoxide (Ph_2S=O) with boranes by the high-valent molybdenum complex MoO_2Cl_2, the ionic transition states corresponding to the heterolytic cleavage of H–B bond requires passing through **TS4** and **TS5** (17.2 kcal/mol, 15.9 kcal/mol for benzamide, 19.3 kcal/mol, 19.7 kcal/mol for N-(diphenylmethylene)benzenamine), 21.3 kcal/mol, 18.3 kcal/mol for diphenyl sulfoxide (Ph_2S=O), Figure 1), and the [2+2] addition reaction of H–B bond into the Mo=O bond needs to pass through **TS7** (27.6 kcal/mol) (**TS11**, 24.0 kcal/mol). The ionic transition states of **TS4**, **TS5** lie lower in energy than the [2+2] addition transition state **TS7** (**TS11**) by 6 ~ 10 kcal/mol for benzamide and N-(diphenylmethylene)benzenamine, and diphenyl sulfoxide. Therefore, we would expect that heterolytic cleavage of H–B bond upon the organic substrates attacks should occur preferentially. And this is the case with benzamide and N-(diphenylmethylene)benzenamine. Whereas, owe to a much higher activation free energy is required for the hydride in the anionic molybdenum hydride $[MoO_2(H)Cl_2]^-$ transfers to the sulfoxide oxygen atom (**TS6**(**Ph_2S=O**), 38.8 kcal/mol), the ionic outer-sphere mechanistic pathway became less favorable with diphenyl sulfoxide (Ph_2S=O) compared to the [2+2] addition pathway. Furthermore, with substrate of benzonitrile, owe to the highest activation free energy barrier is required for migration insertion step (33.8 kcal/mol,**TS9**) along the [2+2] addition pathway, the ionic outer-sphere mechanistic pathway (**TS4**, **TS5** and **TS6**, 23.4, 29.9 and 30.6 kcal/mol) is therefore more favorable.

Conclusions

In summary, DFT calculations with the M06 functional were performed to investigate the reaction mechanism of reduction of a series of organic substrates (amide, amine, nitrile and sulfoxide) with boranes by the high-valent di-oxo molybdenum complex MoO_2Cl_2. Two proposed mechanisms are considered: the ionic outer-sphere pathway involving the

organic substrates nucleophilic attack at the borane center in the η^1-borane molybdenum complex, which results in heterolytic cleavage of the B−H bond; and the [2+2] addition mechanism involving the addition of the B–H bond across the metal oxo Mo=O bonds, and the rate-determining steps in each case were determined. By comparing the energetics of the ionic outer-sphere mechanistic pathway and the [2+2] addition mechanism pathway for the MoO_2Cl_2-catalyzed reduction of benzamide, N-(diphenylmethylene)benzenamine, benzonitrile, and diphenyl sulfoxide with boranes,, the activation free energy barriers for the ionic outer-sphere mechanistic pathway are 22.7 kcal/mol, 19.7 kcal/mol, and 30.6 kcal/mol for substrates of benzamide, N-(diphenylmethylene)benzenamine and benzonitrile, respectively, which is 4.9 kcal/mol, 7.9 kcal/mol and 3.2 kcal/mol more favorable than the [2+2] addition pathway. However, for diphenyl sulfoxide, the [2+2] addition mechanistic pathway is the preferable pathway, being 14.8 kcal/mol lower than the ionic outer-sphere mechanistic pathway.

Along the ionic outer-sphere mechanistic catalytic cycle, the metal center acts as Lewis acid to render the bound B–H group more polarized and more susceptible to nucleophilic attack by the organic substrate. It is worth mentioning that our calculations show that the multiply bonded oxo ligand in the high-valent di-oxo-molybdenum(VI) complex MoO_2Cl_2 does not participate in the activation of the B–H bond along the ionic outer-sphere mechanistic pathway, which is contrast to the [2+2] addition mechanism involving the addition of the B–H bond across the metal oxo bond. The current study provides a greater understanding of X–H bond activation along with further mechanistic insights into the mechanism of reduction by transition-metal complexes in high-oxidation states. Our results highlight that high-valent transition metal complexes can act as Lewis acids to catalyze reduction reactions.

Acknowledgements

We acknowledge the support of the National Natural Science Foundation of China (No. 21103093), a Project Funded by the Priority Academic Program Development of Jiangsu Higher Education Institutions, and a Project Funded by Foundation of Jiangsu Collaborative Innovation Center of Biomedical Functional Materials. We also thank the Shanghai Supercomputer Center and the Nanjing University HPCC for their technical support.

Notes and references

Jiangsu Collaborative Innovation Center of Biomedical Functional Materials, Jiangsu Provincial Key Laboratory for NSLSCS, College of Chemistry and Materials Science, Nanjing Normal University, Nanjing
E-mail: weihaiyan@njnu.edu.cn
[§] *These authors contributed equally*

Electronic Supplementary Information (ESI) available: [Complete Ref. 28, the comparison of different basis set levels, additional results not shown in the text, and Cartesian coordinates of all optimized structures discussed in the paper].

1 (a) Brown, H. C. Hydroboration; Wiley-Interscience: New York, **1962**. (b) Pelter, A.; Smith, K.; Brown, H. C. Borane Reagents; Academic Press: New York, **1988**. (c) Burgess, K.; Ohlmeyer, M. J. *Chem. Rev*. **1991**, *91*, 1179.

2 (a) Fu, G. C.; Evans, D. A. *J. Org. Chem*. **1990**, *55*, 5678. (b) Oshima, K.; Ohmura, T.; Suginome, M. *J. Am. Chem. Soc*. **2012**, *134*, 3699. (c) Musaev, D. G.; Mebel, A. M.; Morokuma, K. *J. Am. Chem. Soc*. **1994**, *116*, 1839. (d) Yang, Z.; Pal, R.; Hoang, G. L.; Zeng, X.; Takacs, J. M. *ACS Catal*. **2014**, *4*, 763. (e) Feng, X.; Jeon, H.; Yun, J. *Angew. Chem. Int. Ed*. **2013**, *52*, 3989. (f) Crudden, C. M.; Edwards, D. *Eur. J. Org. Chem*. **2003**, *24*. 4695. (g) Glasspoole, B. W.; Ghozati, K.; Moir, J. W.; Crudden, C. M. *Chem. Commun*. **2012**, *48*, 1230. (h) Farmer, J. L.; Hunter, H. N.; Organ, M. G. *J. Am. Chem. Soc*. **2012**, *134*, 17470. (i) Cazorla, C.; Métay, E.; Lemaire, M. *Tetrahedron* **2011**, *67*, 8615.

3 (a) Lee, C.; Zhou, J.; Ozerov, O. V. *J. Am. Chem. Soc*. **2013**, *135*, 3560. (b) Crabtree, R. H.; Davis, M. W. *J. Org. Chem*. **1986**, *51*, 2655. (c) Hayashi, T.; Matsumoto, Y.; Ito, Y. *J. Am. Chem. Soc*. **1989**, *111*, 3426. (d) Semba, K.; Shinomiya, M.; Fujihara, T.; Terao, J.; Tsuji, Y. *Chem. –Eur. J*. **2013**, *19*, 7125. (e) Crudden, C. M.; Hleba, Y. B.; Chen, A. C. *J. Am. Chem. Soc*. **2004**, *126*, 9200. (f) Neilson, B. M.; Bielawski, C. W. *Organometallics* **2013**, *32*, 3121. (g) Evans, D. A.; Fu, G. C.; Hoveyda, A. H. *J. Am. Chem. Soc*. **1992**, *114*, 6671.

4 (a) Oluyadi, A. A.; Ma, S.; Muhoro, C. N. *Organometallics* **2013**, *32*, 70. (b) Almqvist, F.; Torstensson, L.; Gudmundsson, A.; Frejd, T. *Angew. Chem. Int. Ed*. **1997**, *36*, 376. (c) Giffels, G.; Dreisbach, C.; Kragl, U.; Weigerding, M.; Waldmann, H.; Wandrey, C. *Angew. Chem. Int. Ed.* **1995**, *34*, 2005. (d) Le, H.; Kyne, R. E.; Brozek, L. A.; Morken, J. P. *Org. Lett*. **2013**, *15*, 1432. (e) Mlynarski, S. N.; Karns, A. S.; Morken, J. P. *J. Am. Chem. Soc*. **2012**, *134*, 16449.

5 (a) Yuan, Y.; Wang, X.; Li, Y.; Fan, L.; Xu, X.; Chen, Y.; Li, G.; Xia, W. *Organometallics* **2011**, *30*, 4330. (b) Matsuda, N.; Hirano, K.; Satoh, T.; Miura, M. *J. Am. Chem. Soc*. **2013**, *135*, 4934. (c) Partridge, B. M.; Chausset-Boissarie, L.; Burns, M.; Pulis, A. P.; Aggarwal, V. K. *Angew. Chem. Int. Ed*. **2012**, *51*, 11795.

6 Sousa, S. C.A.; Cabrita, I.; Fernandes, A. C. *Chem. Soc. Rev*. **2012**, *41*, 5641.

7 (a) Nolin, K. A.; Ahn, R. W.; Kobayashi, Y.; Kennedy-Smith, J. J.; Toste, F. D. *Chem. –Eur. J.* **2010**, *16*, 9555. (b) Blanc, A.; Toste, F. D. *Angew. Chem. Int. Ed*. **2006**, *45*, 2096. (c) Nolin, K. A.; Krumper, J. R.; Puth, M. D.; Bergman, R. G.; Toste, F. D. *J. Am. Chem. Soc*. **2007**, *129*, 14684.

8 (a) Ison, E. A.; Corbin, R. A.; Abu-Omar, M. M. *J. Am. Chem. Soc*. **2005**, *127*, 11938. (b) Du, G. D.; Fanwick, P. E.; Abu-Omar, M. M. *J. Am. Chem. Soc*. **2007**, *129*, 5180. (c) Ison, E. A.; Cessarich, J. E.; Du, G.; Fanwick, P. E.; Abu-Omar, M. M. *Inorg. Chem*. **2006**, *45*, 2385. (d) Abbina, S.; Bian, S.; Oian, C.; Du, G. D. *ACS Catal*. **2013**, *3*, 678. (e) Corbin, R. A.; Ison, E. A.; Abu-Omar, M. M. *Dalton Trans*. **2009**, 2850.

9 (a) Fernandes, A. C.; Fernandes, R.; Romão, C. C.; Royo, B. *Chem. Commun*. **2005**, 213. (b) Royo, B.; Romão, C. C. *J. Mol. Catal. A: Chem*. **2005**, *236*, 107. (c) Reis, P. M.; Romão, C. C.; Royo, B. *Dalton Trans*. **2006**, 1842. (d) Costa, P. J.; Romão, C. C.;

Fernandes, A. C.; Royo, B.; Reis, P. M.; Calhorda, M. J. *Chem. –Eur. J*. **2007**, *13*, 3934. (e) Reis, P. M.; Royo, B. *Catal. Commun*. **2007**, *8*, 1057.

10 (a) Peterson, E.; Khalimon, A. Y.; Simionescu, R.; Kuzmina, L. G.; Howard, J. A. K.; Nikonov, G. I. *J. Am. Chem. Soc*. **2009**, *131*, 908. (b) Gutsulyak, D. V.; Vyboishchikov, S. F.; Nikonov, G. I. *J. Am. Chem. Soc*. **2010**, *132*, 5950. (c) Shirobokov, O. G.; Kuzmina, L. G.; Nikonov, G. I. *J. Am. Chem. Soc*. **2011**, *133*, 6487.

11 (a) Fernandes, A. C.; Romão, C. C. *Tetrahedron Lett*. **2005**, *46*, 8881. (b) R. G. Noronha.; C. C. Romão.; A. C. Fernandes. *Catal. Commun*. **2011**, *12*, 337.

12 Fernandes, A. C.; Romão, C. C. *J. Mol. Catal. A*: *Chem*. **2007**, *272*, 60.

13 Fernandes, A. C.; Romão, C. C. *J. Mol. Catal. A: Chem*. **2006**, *253*, 96.

14 (a) Sousa, A.; Fernandes, A. C. *Tetrahedron Lett*. **2009**, *50*, 6872. (b) Fernandes, A. C.; Romão, C. C. *Tetrahedron lett*. **2007**, *48*, 9176. (c) Fernandes, A. C.; Fernandes, J. A. Romão, C. C.; Veiros, L. F.; Calhorda, M. J. *Organometallics* **2010**, *29*, 5517. (d) Calhorda, M. J.; Costa, P. J. *Dalton Trans.* **2009**, 8155.

15 (a) Fernandes, A. C.; Romão, C. C. *Tetrahedron*. **2006**, *62*, 9650. (b) Reis, P. M.; Royo, B. *Tetrahedron Lett*. **2009**, *50*, 949.

16 (a) Chalk, A. J.; Harrod, J. F. *J. Am. Chem. Soc*. **1965**, *87*, 16. (b) Ojima, I.; Nihonyanagi, M.; Nagai, Y. *J. Chem. Soc. Chem. Commun*. **1972**, 938. (c) Ojima, I.; Nihonyanagi, M.; Kogure, T.; Kumagai, M.; Horiuchi, S.; Nakatsugawa, K.; Nagai, Y. *J. Organomet. Chem*. **1975**, *94*, 449. (d) Corey, J. Y.; Braddock-Wilking, J. *Chem. Rev*. **1999**, *99*, 175. (e) Corey, J. Y. *Chem. Rev*. **2011**, *111*, 863. (f) Murai, T.; Sakane, T.; Kato, S. *J. Org. Chem*. **1990**, *55*, 449. (g) Riener, K.; Högerl, M. P.; Gigler, P.; Kühn, F. E. *ACS Catal.* **2012**, *2*, 613. (h) Ojima, I.; Kogure, T.; Kumagai, M.; Horiuchi, S.; Sato, T. *J. Organomet. Chem*. **1976**, *122*, 83. (i) Reyes, C.; Prock, A.; Giering, W. P. *Organometallics* **2002**, *21*,546. (j) Zheng, G. Z.; Chan, T. H. *Organometallics* **1995**, *14*, 70. (k) Zheng, J. X.; Darcel, C.; Sortais, J. B.; *Catal. Sci. Technol*. **2013**, *3*, 81.

17 (a) Kennedy-Smith, J. J.; Nolin, K. A.; Gunterman, H. P.; Toste, F. D. *J. Am. Chem. Soc*. **2003**, *125*, 4056. (b) Nolin, K. A.; Ahn, R. W.; Toste, F. D. *J. Am. Chem. Soc*. **2005**, *127*, 12462.

18 (a) Ison, E. A.; Trivedi, E. R.; Corbin, R. A.; Abu-Omar, M. M. *J. Am. Chem. Soc*. **2005**, *127*, 15374. (b) Du, G.; Abu-Omar, M. M. *Organometallics* **2006**, *25*, 4920.

19 Noronha, R. G.; Costa, P. J.; Romão, C. C.; Calhorda, M. J.; Fernandes, A. C. *Organometallics* **2009**, *28*, 6206.

20 Reis, P. M.; Costa, P. J.; Romão, C. C.; Fernandes, J. A.; Calhorda, M. J.; Royo, B. *Dalton Trans.* **2008**, 1727.

21 Chung, L. W.; Lee, H. G.; Lin, Z.; Wu, Y. D. *J. Org. Chem*. **2006**, *71*, 6000.

22 Thiel, W. R. *Angew. Chem. Int. Ed*. **2003**, *42*, 5399.

23 (a) Marks, D.; Strassner, T. *Inorg. Chem*. **2007**, *46*, 10850. (b) Costa, P. J.; Romão, C. C.; Fernandes, A. C.; Roya, B.; Reis, P. M.; Calhorda, M. J. *Chem. –Eur. J*. **2007**, 13, 3934.

24 (a) Kawano, Y.; Hashiva, M.; Shimoi, M. *Organometallics* **2006**, *25*, 4420. (b) Yasue, T.; Kawano, Y.; Shimoi, M. *Angew. Chem. Int. Ed.* **2003**, *42*, 1727. (c) Shimoi, M.; Nagai, S.; Ichikawa, M.; Kawano, Y.; Katoh, K.; Uruichi, M.; Ogino, H. *J. Am. Chem. Soc.* **1999**, *121*, 11704. (d) Kakizawa, T.; Kawano, Y.; Shimoi, M. *Organometallics* **2001**, *20*, 3211. (e) Crabtree, R. H. *Angew. Chem., Int. Ed. Engl.* **1993**, *32*, 789.

25 Nagaraja, C. M.; Parameswaran, P.; Jemmis, E. D.; Jagirdar, B. R. *J. Am. Chem. Soc*. **2007**, *129*, 5587.

26 (a) Welch, G. C.; Stephan, D. W.; *J. Am. Chem. Soc*. **2007**, *129*, 1880. (b) Castro, C. E.; Stephens, R. D. *J. Am. Chem. Soc*. **1964**, *86*, 4358. (c) Parks, D. J.; Piers, W. E.; Parvez, M.; Atencio, R.; Zaworotko, M. J. *Organometallics* **1998**, *17*, 1369. (d) Blackwell, J. M.; Sonmor, E. R.; Scoccitti, T.; Piers, W. E. *Org. Lett*. **2000**, *2*, 3921. (e) Berkefeld, A.; Piers, W. E.; Parvez, M. *J. Am. Chem. Soc*. **2010**, *132*, 10660. (f) Stephan, D. W.; Erker, G. *Chem. Sci*. **2014**, *5*, 2625. (g) Stephan, D. W. *Org. Biomol. Chem*. **2012**, *10*, 5740. (h) Stephan, D. W. *Dalton Trans.* **2009**, 3129. (k) Stephan, D. W. *Org. Biomol. Chem.* **2008**, *6*, 1535. (i) Chase, P. A.; Stephan, D. W. *Angew. Chem., Int. Ed*. **2008**, *47*, 7433. (j) Ramos, A.; Lough, A. J.; Stephan, D. W. *Chem. Commun.* **2009**, 1118. (k) Geier, S. J.; Gille, A. L.; Gilbert, T. M.; Stephan, D. W. *Inorg. Chem*. **2009**, *48*, 10466.

27 (a) Yan, Z.; Truhlar, D. G. *J. Phys. Chem. A*. **2008**, *112*, 6794. (b) Denis, J.; Eric, A.; Carlo, A.; Rosendo, V.; Yan, Z.; Truhlar, D. G. *J. Chem. Theory. Comput*. **2010**, *6*, 2071.

28 Frisch, M. J. *et. al*. Gaussian 09, Revision A.02, Gaussian, Inc., Wallingford CT, **2009.**

29 (a) Hay, P. J.; Wadt, W. R. *J. Chem. Phys.* **1985**, *82*, 299. (b) Wadt, W. R.; Hay, P. J. *J. Chem. Phys*. **1985**, *82*, 284. (c) Ehlers, A. W.; Böhme, M.; Dapprich, S.; Gobbi, A.; Hoöllwarth, A.; Jonas, V.; Koöhler, K. F.; Stegmenn, R.; Frenking, G. *Chem. Phys. Lett.* **1993**, *208*, 111.

30 Hoöllwarth, A.; Boöhme, M.; Dapprich, S.; Ehlers, A. W.; Gobbi, A.; Jonas, V.; Koöhler, K. F.; Stegmenn, R.; Veldkamp, A.; Frenking, G. *Chem. Phys. Lett*. **1993**, *208*, 237.

31 Marenich, A. V.; Cramer, C. J.; Truhlar, D. G. *J. Chem. Phys. B*. **2009**, *113*, 6378.

32 (a) Weigend, F.; Ahlrichs, R. *Phys. Chem. Chem. Phys*. **2005**, *7*, 3297. (b) Weigend, F. *Phys. Chem. Chem. Phys.* **2006**, *8***,** 1057.

33 CYLview, 1.0b; C. Y. Legault, Université de Sherbrooke, **2009** (http://www.cylview.org).

34 (a) Park, S.; Brookhart, M. *Organometallics* **2010**, *29*, 6057. (b) Parks, D. J.; Piers, W. E. *J. Am. Chem. Soc*. **1996**, *118*, 9440. (c) Parks, D. J.; Blackwell, J. M.; Piers, W. E. *J. Org. Chem*. **2000**, *65*, 3090. (d) Rokob, T. A.; Hamza, A.; Stirling, A.; Soós, T.; Pápai, I. *Angew. Chem., Int. Ed.* **2008**, 47, 2435. (e) Rokob, T. A.; Hamza, A.; Stirling, A.; Pápai, I. *J. Am. Chem. Soc*. **2009**,*131*, 2029.

35 (a) Park, S.; Brookhart, M. *J. Am. Chem. Soc*. **2012**, *134*, 640. (b) Bernskoetter, W. H.; Hanson, S. K.; Brookhart, M. *J. Am. Chem. Soc*. **2009**, 131, 8603. (c) Findlater, M.; Bernskoetter, W. H.; Brookhart, M. *J. Am. Chem. Soc*. **2010**, *132*, 4534. (d) Gu, P.; Wang, W. W.; Wang, Y. O.; Wei, H. Y. *Organometallics* **2013**, *32*, 47. (e) Huang, L. F; Wei, H. Y. *New. J. Chem.* **2014**, *38*, 5421.

36 at M06(BS1) level, which all geometry optimizations were performed under solvent conditions using the SMD continuum model, the transition state **TS4** is 1.2 kcal/mol higher than van der Waals species **3**. However, at the higher-level basis set, BS2, all-electron 6-311++G (2d,p) for nonmetal and quintuple zeta set with extra polarization basis sets (cc-QZVP) for molybdenum, the

transition state **TS4** is calculated to be 1.8 kcal/mol lower than van der Waals species **3**. The observation indicates no stable van der Waals species **3** formed during the ionic outer-sphere pathway.

37 at M06(BS1) level, which all geometry optimizations were performed under solvent conditions using the SMD continuum model, the intermediate **4**(PhC≡N) was calculated to be 2.7 kcal/mol below the transition state **TS4**.

SYNOPSIS TOC (Word Style "SN_Synopsis_TOC").

The multiply bonded oxo ligand does not participate in the activation of the B–H bond with organic substrates of amides, amines, nitriles by the high-valent oxo-molybdenum complex MoO_2Cl_2. Whereas, the [2+2] addition pathway involving the B–H bond of the borane adding across the Mo=O bond is favored with sulfoxides substrate.